ARTICLE

Electronic Stability of Bimetallic $Au_2@Cu_6$ Nanocluster: Closed-Shell Interaction and Multicenter Bonding

Ying-ying Ma[a], Yuan-qin Yu[b*], Long-jiu Cheng[a,c*]

a. Department of Chemistry, Anhui University, Hefei 230601, China
b. School of Physics and Materials Science, Anhui University, Hefei 230601, China
c. Anhui Province Key Laboratory of Chemistry for Inorganic/Organic Hybrid Functionalized Materials, Anhui University, Hefei 230601, China

(Dated: Received on November 12, 2019; Accepted on December 16, 2019)

Metallophilic interaction is a unique type of weak intermolecular interaction, where the electronic configuration of two metal atoms is closed shell. Despite its significance in multidisciplinary fields, the nature of metallophilic interaction is still not well understood. In this work, we investigated the electronic structures and bonding characteristic of bimetallic $Au_2@Cu_6$ nanocluster through density functional theory method, which was reported in experiments recently [Angew. Chem. Int. Ed. **55**, 3611 (2016)]. In general thinking, interaction between two moieties of $(CuSH)_6$ ring and $(Au_2PH_3)_2$ in the $Au_2@Cu_6$ nanocluster can be viewed as a d^{10}-σ closed-shell interaction. However, chemical bonding analysis shows that there is a ten center-two electron (10c-2e) multicenter bonding between two moieties. Further comparative studies on other bimetallic nanocluster $M_2@Cu_6$ (M=Ag, Cu, Zn, Cd, Hg) also revealed that multicenter bonding is the origin of electronic stability of the complexes besides the d^{10}-σ closed-shell interaction. This will provide valuable insights into the understanding of closed-shell interactions.

Key words: Multicenter bonding, Density function theory, Closed-shell interaction, Metallophilic interaction, Metallic cluster

I. INTRODUCTION

Weak intermolecular interactions such as hydrogen bond, halogen bond, and van der Waals forces are prevalent in nature and play a crucial role in multidisciplinary field including physics, chemistry, biology and material science [2–5]. Among these, metallophilic interaction is a unique type coined to describe the attractive interaction between metal atoms with closed-shell electronic configuration [6–11], such as two gold atoms in the +1 oxidation state Au(I), *i.e.* $5d^{10}$-$5d^{10}$ [12–14]. It was shown that the equilibrium distances between the atoms of metallophilic interaction are in the range of 2.50–3.50 Å [15] and the interaction energy can be up to 12 kcal/mol, much weaker than covalent bonds but stronger than van der Waals bonds, even be comparable with strong hydrogen bonds [16]. The significance of metallophilic interactions in the stabilization of three-dimensional structure of new materials, molecular recognition phenomenon, crystal packing, stereoselectivity and supramolecular chemistry has been well documented [17].

Recently, the existence of dative bonding between closed-shell atoms (BeF^-) has been reported [18–20]. For aurophilic interaction, no one has tried to explain it from a perspective of chemical bonding due to its closed-shell property. Lately, there is an upsurge of interest for the description of the chemical bond through multicenter bonding method. As a special covalent bond, multicenter bonding has been a popular chemistry language to unravel the unique electronic structure and physical/chemical property of various compounds. For example, multicenter bond method has been recently used as a new measurement of superatom-superatom bonding [21]. Despite that aurophilic interaction cannot be validated by a conventional localized chemical bond, it is possible to be rationalized from delocalized bond.

Recently, Zhu group synthetized an interesting bimetallic $Au_2@Cu_6$ nanocluster [1]. This cluster has a hexagonal $(CuSR)_6$ framework aggregated by two gold atoms, and the two gold atoms are further capped by two ligands L such as PR_3. In this compound, the $(CuSR)_6$ ring is a stable moiety with $3d^{10}$ closed-shell configuration on Cu atom, whereas the $Au_2@L_2$ is another stable moiety with σ orbital between the two Au atoms. When the $Au_2@L_2$ is inserted into Cu_6 ring, two moieties are bound together with d^{10}-σ closed-shell interaction. We investigated the electronic structures

Authors to whom correspondence should be addressed. E-mail: clj@ustc.edu.cn, yyq@ahu.edu.cn

and chemical bonding by first principle calculations in $Au_2@Cu_6$ nanoclusters to decipher its bonding nature. Furthermore, in order to make a comparative analysis, the Au atom was substituted with other metal atoms (M) such as silver, copper, zinc, chromium and mercury, and the ligand (L) was substituted with other elements such as halogen. The results show that, the ten center two electron (10c-2e) multicenter bonding is also the key issue for the stability of the complexes besides the d^{10}-σ closed-shell interaction.

II. COMPUTATION METHOD

Geometry optimizations are performed using density functional theory (DFT) methods with TPSS-D3 [22–26] functional, which has been proved reliable in the prediction of $Au_m(SR)_n$ nanocluster [27–29], and relativistic effective core potential basis set (def2-tzvp) was used for each atom [30, 31]. The binding energy (E_b) is calculated at the same level, which is defined as E_b=E_{ring}+$E_{monomer}$–$E_{complex}$, where E_{ring}, $E_{monomer}$ and $E_{complex}$ are the energies of $(CuSH)_6$ hexatomic ring, monomer, and complex, respectively. Adaptive natural density partitioning (AdNDP) method is chosen for the chemical bonding analysis of the complexes [32–34]. The method was developed by Zubarev and Boldyrev, which has been successfully applied in a number of systems [35]. AdNDP is based on the concept of the electron pair as the main element of chemical bonding models, which recovers both Lewis bonding elements (1c-2e and 2c-2e objects) and delocalized bonding elements (*n*c-2e) [33, 36–38]. It is consistent with the recent developed electron density of delocalized bonds (EDDB) method [39], which is a powerful tool for deciphering the multicenter bonding in molecules and clusters with delocalized electrons [40, 41]. The extended transition state natural orbitals for chemical valence (ETS-NOCV [42]) with the ADF 2014 package [43] were employed for analyzing the interactions in all complexes at the TPSS-D3/TZ2P level of theory. Electron localized function (ELF) method describes the features of bonding in terms of the local kinetic energy, which is approximately expressed as a function of electron density and its first and second derivatives [44–48]. In this work, ELF analysis was carried on for further discussion of their electronic structures. All calculations were carried out using the Gaussian 09 package, and the molecular visualization was performed using MOLEKEL 5.4 [49, 50].

III. RESULTS AND DISCUSSION

A. $Au_2@Cu_6$ structure

As mentioned above, Zhu group [21] reported a significant fluorescence enhancement material, its crystal structure was successfully determined as $(AuPPh_2Py)_2(CuSC_{10}H_{15})_6$ by X-ray crystallography recently. This nanocluster has a $Au_2@Cu_6$ metal core with hexagonal $(CuSR)_6$ framework aggregated by two gold atoms. To simply the calculation, here we use $(CuSH)_6$ to substitute $(CuSR)_6$ and PH_3 to PPh_2Py. Previous calculations showed that such substitutions do not significantly affect electronic structures of the compound. FIG. 1 shows the optimized structures of $(AuPH_3)_2@(CuSH)_6$ cluster calculated at TPSS-D3/def2-tzvp level. The calculated Au–Au (2.619 Å) and Cu–S (2.272 Å) bond lengths are very close to the experimental values (2.583 Å and 2.213 Å). The distance between the Au in the monomer and Cu in the ring is 2.907 Å (experiment 3.051 Å), much shorter than the sum of van der Waals radius. The calculated binding energy of complex $Au_2@Cu_6$ is –113.82 kcal/mol, much higher than the value of general closed-shell interactions. To investigate the interaction in $Au_2@Cu_6$ cluster more clearly, the structures of monomers Au_2, $(AuPH_3)_2$ and hexagonal $(CuSH)_6$ ring were also calculated. Both monomers and complexes have no imaginary frequency with fairly large HOMO–LUMO gaps between 1.88 and 3.19 eV, indicating certain stability. Clearly, the Au–Au bond and S–Cu bonds are slightly elongated in the complex compared to that in the monomer (as labeled in FIG. 1). These small geometric changes indicated that there were closed-shell interactions in the complex when the monomer inserted hexagonal ring.

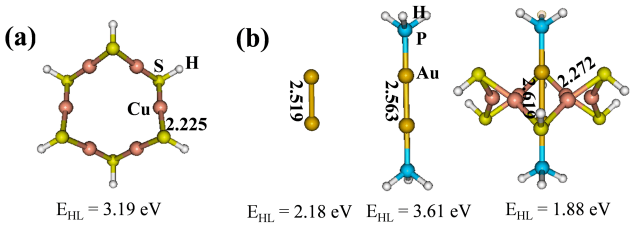

FIG. 1 Optimized structures of (a) hexagonal $(CuSH)_6$ moiety and (b) $(AuPH_3)_2(CuSH)_6$ complexes at the TPSSTPSS-D3/def2-TZVP level. The bond lengths are labeled in Å. E_{HL} gives the HOMO–LUMO gaps. For color image, see the online version.

B. Chemical bonding analysis

The interaction between Au_2 and Cu_6 ring is rather strong, and there should exist other interactions besides the closed-shell interaction. To gain direct insights into the interaction between monomer and Cu_6 ring framework, we applied AdNDP method to obtain patterns of chemical bonding. FIG. 2 shows a full AdNDP analysis on the monomer and complex. It can be seen that there are five $5d^{10}$ lone pairs (LPs) on each Au atom with ON=1.94–2.00 |e| (only shown in one Au atom), ON means the occupancy number of electrons, six 2c-

DOI:10.1063/1674-0068/cjcp1912200

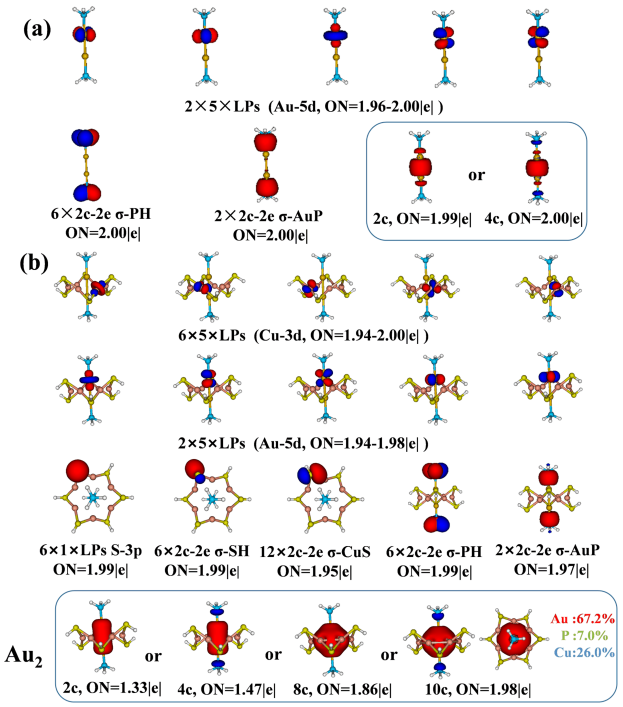

FIG. 2 AdNDP chemical bonding analysis for (a) $(AuPH_3)_2$ monomer and (b) $(AuPH_3)_2@(AuSH)_6$ complex. For color image, see the online version.

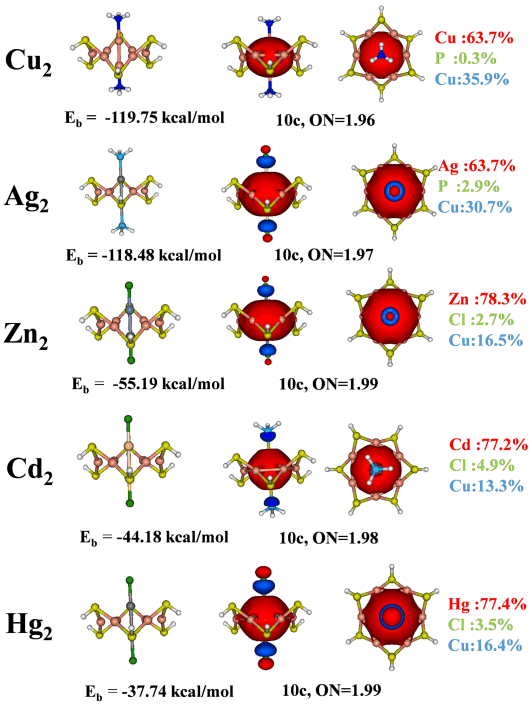

FIG. 3 AdNDP chemical bonding analysis for the multicenter bond (10c-2e) of $M_2@Cu_6$. Cu_2:$(CuNH_3)_2@(CuSH)_6$, Ag_2:$(AgPH_3)_2@(CuSH)_6$, Zn_2:$(ZnCl)_2@(CuSH)_6$), Cd_2:$(CdCl)_2@(CuSH)_6$), Hg_2:$(CdCl)_2@(CuSH)_6$). E_b gives the binding energy. For color image, see the online version.

2e localized P–H bonds with ON=2.00 |e|, two 2c-2e localized Au–P bonds with ON=2.00 |e|, and one 2c-2e localized Au–Au bond with ON=1.99 |e| (FIG. 2(a)) for $(AuPH_3)_2$ monomer. In addition, AdNDP analysis reveals that the Au–Au bond can be considered as 4c-2e delocalized multicenter bond in the $(AuPH_3)_2$ monomer with ON=2.00 |e|.

For the complex $Au_2@Cu_6$, AdNDP analysis shows that there are thirty lone pairs on six Cu atom with ON=1.94–1.98 |e|, ten LPs on two Au atoms with ON=1.94–2.00 |e|, and six LPs on the six S atoms with ON=1.99 |e|, six 2c-2e localized S–H bonds with ON=1.99 |e| and twelve 2c-2e localized Cu–S bonds with ON=1.95 |e|, six 2c-2e localized P–H bonds, and two 2c-2e localized Au–P bonds (FIG. 2(b)). All above AdNDP analysis is consistent with the assignment of valence electrons of $Au_2@Cu_6$. However, ON value is only 1.33 |e| if it was regarded as a localized 2c-2e bond for the Au–Au bond. Such a low ON value is obviously unreasonable for a chemical bond. So we analyzed the Au–Au bond in the complex by considering it as 4c-2e (Au_2P_2), 8c-2e ($Au_2@Cu_6$) or 10c-2e ($Au_2P_2Cu_6$) multicenter bonding, and their corresponding ON are 1.47 |e|, 1.86 |e|, and 1.98 |e|, respectively. Therefore, the 10c-2e multicenter bond is a more reasonable way of bonding between the monomer and $(CuSH)_6$ ring since its ON is close to the ideal 2.00 |e|. The electronic contributions for Au, P, and Cu atoms in the delocalized 10c-2e bond are 67.2%, 7.0%, and 26.0%, respectively.

Apart from $Au_2@Cu_6$, other bimetal clusters $M_2@Cu_6$ were also investigated, in which the Au atom was substituted with the same group Ag and Cu atoms or main group metal Zn, Cd, and Hg atoms, and the ligands PH_3 are substituted with NH_3 or Cl_2. The calculated results show that these substituted nanoclusters are also stable. Therefore, the bimetal clusters with $M_2@Cu_6$ core may commonly exist. The calculated binding framework and bonding pattern of other $M_2@Cu_6$ nanoclusters are similar to $Au_2@Cu_6$. The detailed AdNDP analyses are listed in supplementary materials. Here, we only show their bonding pictures of 10c-2e multicenter bond, as shown in FIG. 3. It is clear that all the ON values of 10c-2e delocalized bond are close to 2.00 |e|, indicating that there is a 10c-2e multicenter bond in each $M_2@Cu_6$ nanocluster.

To reveal the nature of 10c-2e multicenter bond in each complexes, the percentages of electrons located on M, L and Cu atom were calculated. The value in red is from two M atoms in monomer (M=Cu, Ag, Zn, Cd, Hg), and the value in green is from two P, N, or Cl atoms in ligands, and the value in blue is from six Cu atoms in the Cu_6 ring. For example, the percentage of electron on two Ag atoms is 63.7% in $Ag_2@Cu_6$ complex, and the percentage of electron on two P atoms of ligand and six Cu atoms of ring are 2.9% and 30.7%, respectively. This indicates that the electron is delocal-

DOI:10.1063/1674-0068/cjcp1912200

ized away from σ_{Ag-Ag}, and partly enters orbitals of Cu atoms in hexagonal ring and partly enter into σ^*_{Ag-P} orbital, forming 10c-2e multicenter bonding in $Ag_2@Cu_6$. For M=Au, Ag, and Cu, the percentage of electron on six Cu atoms is larger than that for group 12 metals (Zn, Cd, Hg), and so the percentage of electron on two M atoms changes in reverse trend. For M=Au, Ag, and Cu, the percentage in M (63.7%–67.2%) is obvious lower than that for M=Zn, Cd, Hg (77.3%–78%). This indicates that delocalization of the σ_{M-M} bond is greater for M=Au, Ag, and Cu. Thus, there is a stronger 10c-2e multicenter bond in complex of group 11 metals, consistent with the sequence of the calculated binding energy for $M_2@Cu_6$. This can be attributed to the fact that the electrons are easier to be delocalized when the metal is more active. It should be mentioned that there is an anomaly that the electron located on six Cu atoms is larger in $Hg_2@Cu_6$ (16.4%) than that in $Cd_2@Cu_6$ (13.3%). This can be explained by the fact that the Hg atom is too large, and actually its binding energy is the smallest in all complexes. From above, it can be seen that the nature of 10c-2e multicenter bond in $M_2@Cu_6$ is a consequence of electron transfer between σ_{M-M} bond and the orbital of Cu atom. The $M_2@Cu_6$ clusters are bound together with two stable moieties through multicenter bonds. Cu atom in the Cu_6 ring is between sp and sp^2, and the nature of the multicenter bond is the delocalization of σ_{M-M} electron over the empty sp-sp^2 orbitals.

C. $X_2@Cu_6$ structure

To expand the bimetal nanocluster $M_2@Cu_6$ to the case of nonmetal atoms, we constructed a series of complexes $X_2@Cu_6$ (X=F, Cl, Br, I). As expected, the designed complexes are real local minimum structures without imaginary frequency except for $F_2@Cu_6$. To study the relative stability of $X_2@Cu_6$ complexes, we scanned their binding energy versus the vertical distance between bottom of monomer (X_2) and center of hexagonal ring, along with the variation trend of the binding energy of $Zn_2@Cu_6$ as a contrast (as shown in FIG. 4). There is a deep well with negative binding energy for $Zn_2@Cu_6$, indicating high stability (FIG. 4(a)). The binding energy of $X_2@Cu_6$ cluster (X=F, Cl, Br, I) is smaller than $M_2@Cu_6$. However, it still has a minimum except for F_2 monomer, indicating that $X_2@Cu_6$ (X=Cl, Br, I) can also be stable, especially for the case of X=I, which has the lowest value among all the halogen atoms. This is due to the fact that I–I bond is easier to be polarized and the interaction between X_2 and Cu_6 ring becomes stronger, leading to a stronger multicenter bond between two moieties. As for the F_2 monomer, F atom is unwilling to share its electrons with other atoms due to large electronegativity. There is little electron transfer from σ_{F-F} orbital to Cu_6 ring, leading to instability with an imaginary frequency.

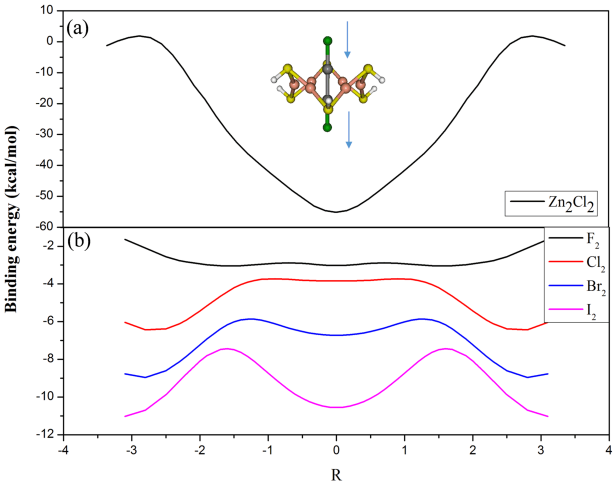

FIG. 4 The variation trend of binding energies with the vertical distance between two units in (a) $(ZnCl)_2@(CuSH)_6$; and (b) $X_2@(CuSH)_6$ (X=F, Cl, Br, I). R is distance between the center of monomer and the center of the hexagonal ring. For color image, see the online version.

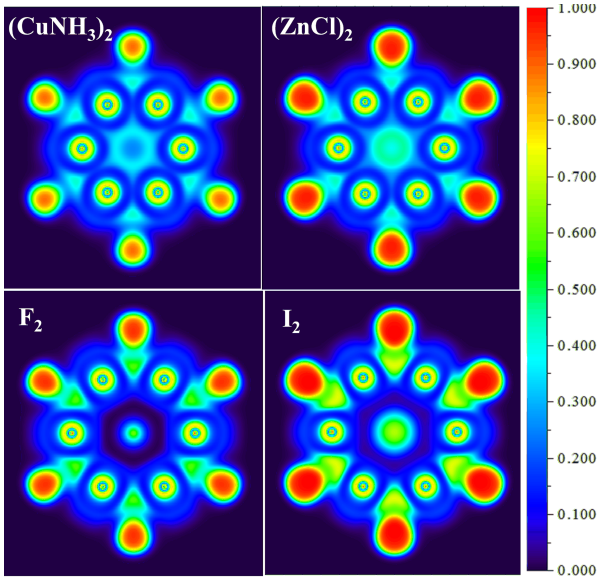

FIG. 5 ELF contour for $(ML)_2@(CuSH)_6$ complexes (M=Cu, Ag, and Au). The color scale for the values is given on the right of the figure. For color image, see the online version.

D. ELF analysis

ELF results provide electronic density distribution in the cross section of the complexes in color and shape and further insights into molecular interaction can be obtained. From the result of ELF analysis, the delocalization of electrons is clearly resolved. FIG. 5 presents ELF analysis of $Cu_2@Cu_6$, $Zn_2@Cu_6$, $F_2@Cu_6$ and $I_2@Cu_6$ complexes. For ELF cut plane, the relative value is within the range of (0,1), in which the highest value of 1.0 with red color represents the full delocal-

DOI:10.1063/1674-0068/cjcp1912200

TABLE I Energy decomposition analysis results (in kJ/mol) between the hexagonal ring Cu_6 and the monomer in the $M_2@Cu_6$ complexes (M=Cu, Ag, Au, Zn, Cd, Hg)[a].

Complex	$\Delta E_{\rm int}$	$\Delta E_{\rm Pauli}$	$\Delta E_{\rm elstat}$	$\Delta E_{\rm orb}$	$\Delta E_{\rm disp}$
$(CuNH_3)_2@(CuSH)_6$	–123.69	389.96	–348.89 (68%)	–144.89 (28%)	–19.86 (4%)
$(AgPH_3)_2@(CuSH)_6$	–119.72	376.24	–325.96 (66%)	–132.39 (27%)	–37.61 (8%)
$(AgNH_3)_2@(CuSH)_6$	–116.36	384.87	–337.55 (67%)	–129.79 (26%)	–33.90 (7%)
$(AgCO)_2@(CuSH)_6$	–110.44	362.52	–308.79 (65%)	–130.63 (28%)	–33.53 (7%)
$(AuPH_3)_2@(CuSH)_6$	–117.31	344.81	–292.45 (63%)	–125.82 (27%)	–43.85 (9%)
$(ZnF)_2@(CuSH)_6$	–49.49	219.13	–149.50 (56%)	–104.39 (39%)	–14.72 (5%)
$(ZnCl)_2@(CuSH)_6$	–59.00	226.59	–155.43 (54%)	–110.62 (39%)	–19.54 (7%)
$(ZnBr)_2@(CuSH)_6$	–64.37	230.00	–158.42 (54%)	–114.45 (39%)	–21.50 (7%)
$(ZnI)_2@(CuSH)_6$	–70.22	235.34	–163.28 (53%)	–118.92 (39%)	–23.37 (8%)
$(ZnSiH_3)_2@(CuSH)_6$	–79.49	239.00	–175.52 (55%)	–120.08 (36%)	–22.89 (7%)
$(CdCl)_2@(CuSH)_6$	–48.26	227.14	–156.79 (57%)	–99.62 (38%)	–19.00 (7%)
$(HgCl)_2@(CuSH)_6$	–41.60	203.27	–140.16 (57%)	–82.43 (34%)	–22.28 (9%)

[a] The data obtained at the TPSS-D3/TZ2P level of theory.

ization of electron and strong interaction, whereas the smallest value of 0.0 with blue color represents the no delocalization of electron and weak interaction. It can be seen that the electron delocalization of the complexes follows the order of $\sigma_{\rm Cu-Cu}>\sigma_{\rm Zn-Zn}>\sigma_{\rm I-I}>\sigma_{\rm F-F}$. The electron delocalization of $\sigma_{\rm Cu-Cu}$ bond is the most obvious, and almost no delocalization of $\sigma_{\rm F-F}$ bond can be observed. Therefore, the interaction between $\sigma_{\rm Cu-Cu}$ monomer and Cu_6 ring is the strongest, while there is no obvious covalent interaction between $\sigma_{\rm F-F}$ and Cu_6 ring. The ELF results are consistent with the results of binding energy and chemical bonding analysis.

E. Energy decomposition analysis (EDA)

To get a closer insight into the nature of the interaction between the fragments in the studied complexes, ETS-NOCV [42] has been carried out at the TPSS-D3/TZ2P level of theory. The interaction energy between the fragments ($\Delta E_{\rm int}$) in ETS-NOCV is divided into four physically meaningful components: Pauli repulsion ($\Delta E_{\rm Pauli}$), electrostatic ($\Delta E_{\rm elstat}$), and orbital ($\Delta E_{\rm orb}$), when a dispersion-corrected functional is employed, dispersion ($\Delta E_{\rm disp}$) is also included. In such a scheme, the interaction energy ($\Delta E_{\rm int}$) is decomposed according to the following equation into the above-mentioned components:

$$\Delta E_{\rm int} = \Delta E_{\rm orb} + \Delta E_{\rm Pauli} + \Delta E_{\rm elstat} + \Delta E_{\rm disp}$$

The results of the energy decomposition analysis between the hexagonal Cu_6 ring and the monomer in the $M_2@Cu_6$ complexes are listed in Table I, and those between the X_2 (X=F, Cl, Br, I) and Cu_6 fragment are presented in Table S1 (supplementary materials). It can be seen that, the values of the calculated $\Delta E_{\rm int}$ for the series of $M_2@Cu_6$ (M=Cu, Ag, Au, Zn, Cr, Hg) complexes decrease from copper to mercury, and the $Cu_2@Cu_6$ complex has the greatest interaction energy. This tendency is consistent with the results of former AdNDP and ELF analyses, which have shown that the degree of delocalization is the highest for $\sigma_{\rm Cu-Cu}$ and the lowest for $\sigma_{\rm Hg-Hg}$.

The contributions of the attractive terms in EDA for each complex are also listed in Table I. The contribution of electrostatic interactions in all complexes is greater than orbital interactions. On the other hand, as expected, the contribution of dispersion forces in all complexes is little (4%–9%).

F. Deformation density analysis

The analysis of deformation density plots provides detailed information on the local or remote orbitals donating and accepting electron density. The deformation density maps for $Cu_2@Cu_6$, $Zn_2@Cu_6$, $I_2@Cu_6$, and $F_2@Cu_6$ are given in FIG. 6, which show clearly that the interaction between M_2 and Cu_6 ring arises from charge transformation, primarily from the $\sigma_{\rm M\text{-}M}$ to Cu_6 ring. It can be seen that the charge transformation of the complexes follows the order of $Cu_2@Cu_6>Zn_2@Cu_6>I_2@Cu_6>F_2@Cu_6$, which is consistent with the results of ELF and chemical bonding analysis. Those for the other studied complexes are given in supplementary materials.

G. Ligand effect

As concluded above, the nature of the multicenter bond is the delocalization of $\sigma_{\rm M-M}$, *i.e.*, electron transformation from $\sigma_{\rm M-M}$ to Cu_6 ring. Therefore, the electron donating ability of ligands will af-

DOI:10.1063/1674-0068/cjcp1912200

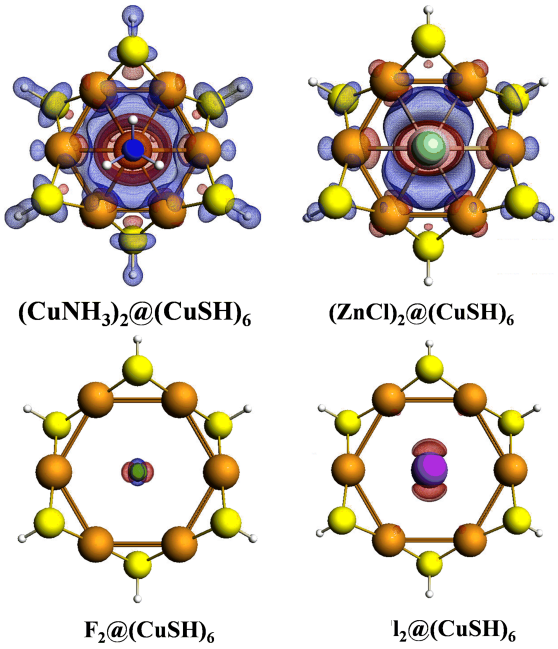

FIG. 6 Contours of deformation densities ($\Delta\pi$=0.001) indicate the flow of electrons, from red to blue, involved in the Cu_6–monomer interactions. For color image, see the online version.

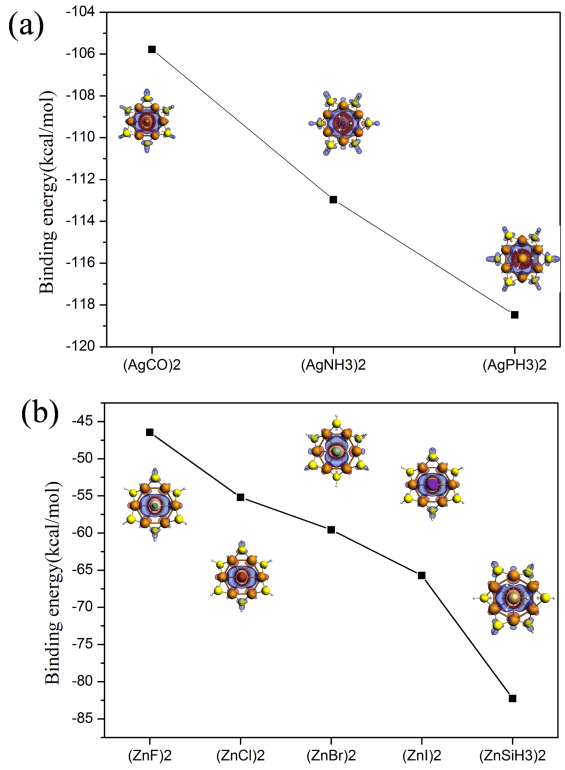

FIG. 7 The variation of binding energies with the different ligands in two systems: (a) $(AgL)_2@(CuSH)_6$ (L=PH_3, NH_3, CO), (b) $(ZnX)_2@(CuSH)_6$ (X=F, Cl, Br, I, SiH_3) systems. Labeled are contours of deformation densities. For color image, see the online version.

fect the strength of multicenter bonds along with the stability of compounds. If the ligands pull electrons, the multicenter bond will be weakened, whereas the ligands give electrons and the multicenter bond will be strengthened. To investigate this issue, we constructed a series of complexes with different kind of ligands, *i.e.* $(AgL)_2@(CuSH)_6$ (L=PH_3, NH_3, CO) and $(ZnX)_2@(CuSH)_6$ (X=F, Cl, Br, I, SiH_3). FIG. 7 presents the changes of their binding energy with different ligands L (the deformation density maps are also labeled). It can be seen that the binding energy of the complexes increases in the following order: PH_3>NH_3>CO and SiH_3>I>Br>Cl>F, consistent with the electron donating ability of the ligand. The binding energy is also consistent with the deformation densities. As can be seen from the deformation density maps, the amount of electron outflow is higher with greater electronegativity of the ligands (PH_3 and SiH_3), resulting in stronger binding energy. It should be noted that, the electron donating ability of the σ orbital of CO is very strong, but the overall electron donation is not too high due to the d→π back donation. Therefore, the ligand plays an important role in the interaction between the monomer and the Cu_6 ring. The stronger the electron donating ability of the ligand is, the stronger the interaction will be. This is the reason that the strong electron donating ability of the ligands is favorable for the formation of delocalized 10c-2e multicenter bonding in $M_2@Cu_6$ nanoclusters.

IV. CONCLUSION

Based on the experimental $Au_2@Cu_6$ compound model, a series of $M_2@Cu_6$ complexes are designed and investigated by DFT methods. The geometrical structures of $M_2@Cu_6$ can be seen as a hexagonal $(CuSH)_6$ framework aggregated by one monomer at the center of outer-loop. From geometries, both M_2 and Cu_6 ring are stable pieces with closed-shell electronic, and the interaction between them seems to be d^{10}-σ closed-shell interaction. However, chemical bonding analyses from AdNDP and ELF methods reveal that the 10c-2e multicenter bonding is responsible for the stability of $M_2@Cu_6$ clusters. Energy scan shows that the curve has a minimum around the equilibrium distance, indicating that the structures were stable. Compared with the binding energy curves of different substitutes, it is found that the electron donating ability plays an important role in the stability of complexes. The nature of the interaction between different types of fragments in the $M_2@Cu_6$ complexes is also investigated with EDA-NOCV. The calculations show that the contribution of electrostatic interactions decreases from copper to mercury. The nature for closed-shell interaction is still not so clear, and the reasons may be different in various

DOI:10.1063/1674-0068/cjcp1912200

systems. This work presents a new view on the d^{10}-σ closed-shell interaction in $M_2@Cu_6$ clusters, where multicenter bonding is the key issue for the stability of the complexes.

Supplementary materials: The detailed AdNDP analyses of all the bimetallic complexes are shown.

V. ACKNOWLEDGEMENTS

This work is supported by the National Natural Science Foundation of China (No.21873001 and No.21873002), and the Foundation of Distinguished Young Scientists of Anhui Province. The calculations are carried out at the High-Performance Computing Center of Anhui University.

[1] X. Kang, S. X. Wang, Y. B. Song, S. Jin, G. D. Sun, H. Z. Yu, and M. Z. Zhu, Angew. Chem. Int. Ed. **55**, 3611 (2016).
[2] A. N. Chernyshev, M. V. Chernysheva, P. Hirva, V. Y. Kukushkin, and M. Haukka, Dalton Trans. **44**, 14523 (2015).
[3] Q. Liu, M. Xie, X. Y. Chang, S. Cao, C. Zou, W. F. Fu, C. M. Che, Y. Chen, and W. Lu, Angew. Chem. Int. Ed. **57**, 6279 (2018).
[4] M. Gil-Moles, M. C. Gimeno, J. M. López-de-Luzuriaga, M. Monge, M. E. Olmos, and D. Pascual, Inorg. Chem. **56**, 9281 (2017).
[5] G. Chen, S. T. Wang, B. Feng, B. Jiang, and M. Miao, Food Chem. **277**, 632 (2019).
[6] R. Echeverría, J. M. López-De-Luzuriaga, M. Monge, S. Moreno, and M. E. Olmos, Inorg. Chem. **55**, 10523 (2016).
[7] P. Pyykkö, Angew. Chem. Int. Ed. **43**, 4412 (2004).
[8] P. Pyykkö, Chem. Soc. Rev. **37**, 1967 (2008).
[9] S. Sculfort and P. Braunstein, Chem. Soc. Rev. **40**, 2741 (2011).
[10] P. K. Mehrotra and R. Hoffmann, Inorg. Chem. **17**, 2187 (1978).
[11] J. Muñiz, C. Wang, and P. Pyykkö, Chem. Eur. J. **17**, 368 (2011).
[12] D. Blasco, J. M. López-de-Luzuriaga, M. Monge, M. E. Olmos, D. Pascual, and M. Rodríguez-Castillo, Inorg. Chem. **57**, 3805 (2018).
[13] Z. Assefa, F. DeStefano, M. A. Garepapaghi, J. H. LaCasce, S. Ouellete, M. R. Corson, J. K. Nagle, and H. H. Patterson, Inorg. Chem. **30**, 2868 (1991).
[14] M. B. Brands, J. Nitsch, and C. F. Guerra, Inorg. Chem. **57**, 2603 (2018).
[15] H. Schmidbaur and A. Schier, Chem. Soc. Rev. **41**, 370 (2012).
[16] P. Pyykkö, Chem. Rev. **97**, 597 (1997).
[17] H. Y. Wang and L. J. Cheng, Nanoscale **9**, 13209 (2017).
[18] A. Kalemos, J. Phys. Chem. A **122**, 8882 (2018).
[19] X. W. Chi, Q. Y. Wu, Q. Hao, J. H. Lan, C. Z. Wang, Q. Zhang, Z. F. Chai, and W. Q. Shi, Organometallics **37**, 3678 (2018).
[20] J. M. López-De-Luzuriaga, M. Monge, M. E. Olmos, and D. Pascual, Organometallics **34**, 3029 (2015).
[21] Q. J. Zheng, C. Xu, X. Wu, and L. J. Cheng, ACS Omega **3**, 14423 (2018).
[22] A. K. Friesen, N. V. Ulitin, S. L. Khursan, D. A. Shiyan, K. A. Tereshchenko, and S. V. Kolesov, Mendeleev Commun. **27**, 374 (2017).
[23] H. Cheng and L. J. Cheng, Comput. Theor. Chem. **1060**, 36 (2015).
[24] L. F. Li, C. Xu, and L. J. Cheng, Comput. Theor. Chem. **1021**, 144 (2013).
[25] Q. Y. Zhang and L. J. Cheng, J. Chem. Inf. Model. **55**, 1012 (2015).
[26] H. Ari, Z. Büyükmumcu, and T. Özpozan, J. Mol. Struct. **1165**, 259 (2018).
[27] S. A. Ivanov, I. Arachchige, and C. M. Aikens, J. Phys. Chem. A **115**, 8017 (2011).
[28] D. E. Jiang, W. Chen, R. L. Whetten, and Z. F. Chen, J. Phys. Chem. C **113**, 16983 (2009).
[29] A. Lechtken, C. Neiss, M. M. Kappes, and D. Schooss, Phys. Chem. Chem. Phys. **11**, 4344 (2009).
[30] Q. M. Liu and L. J. Cheng, J. Alloy Compd. **771**, 762 (2019).
[31] D. W. Szczepanik and J. Mrozek, Comput. Theor. Chem. **1026**, 72 (2013).
[32] Y. J. Cui and L. J. Cheng, RSC Adv. **7**, 49526 (2017).
[33] D. Y. Zubarev and A. I. Boldyrev, Phys. Chem. Chem. Phys. **10**, 5207 (2008).
[34] L. J. Yan, L. J. Cheng, and J. L. Yang, Chin. J. Chem. Phys. **28**, 476 (2015).
[35] D. Y. Zubarev and A. I. Boldyrev, J. Org. Chem. **73**, 9251 (2008).
[36] Y. F. Shen, C. Xu, and L. J. Cheng, RSC Adv. **7**, 36755 (2017).
[37] A. P. Sergeeva and A. I. Boldyrev, Comment. Inorg. Chem. **31**, 2 (2010).
[38] D. Y. Zubarev, D. Domin, and W. A. Lester Jr., J. Phys. Chem. A **114**, 3074 (2010).
[39] D. W. Szczepanik, Comput. Theor. Chem. **1100**, 13 (2017).
[40] D. Szczepanik and J. Mrozek, J. Math. Chem. **51**, 1388 (2013).
[41] D. W. Szczepanik and J. Mrozek, J. Chem. **2013**, 684134 (2013).
[42] G. Frenking and S. Shaik, *The Chemical Bond: Chemical Bonding Across the Periodic Table*, Weinheim: John Wiley & Sons, (2014).
[43] E. J. Baerends, T. Ziegler, J. Autschbach, D. Bashford, A. Bérces, F. Bickelhaupt, C. Bo, P. Boerrigter, L. Cavallo, and D. Chong, *Theoretical Chemistry*, Amsterdam: Vrije Universiteit ADF2014, (2014). http://www.scm.com
[44] B. Silvi, Struct. Chem. **28**, 1389 (2017).
[45] N. K. Nkungli and J. N. Ghogomu, J. Mol. Model. **23**, 200 (2017).
[46] S. Berski and P. Durlak, Polyhedron **129**, 22 (2017).
[47] J. G. Du and G. Jiang, Eur. J. Inorg. Chem. **2016**, 1589 (2016).
[48] A. D. Dergunov, E. A. Smirnova, A. Merched, S. Visvikis, G. Siest, V. V. Yakushkin, and V. Tsibulsky, Biochim. Biophys. Acta **1484**, 14 (2000).
[49] Z. M. Tian and L. J. Cheng, J. Phys. Chem. C **121**, 20458 (2017).
[50] M. Huang, C. Xu, and L. J. Cheng, Acta Chim. Sin. **74**, 758 (2016).

DOI:10.1063/1674-0068/cjcp1912200

Supplementary information

Electronic stability of the bimetallic Au_2Cu_6 nanoclusters: closed-shell interaction and multicenter bonding

Yingying Ma,[a] Yuanqin Yu,*[b] Longjiu Cheng*[ac]

[a]Department of Chemistry, Anhui University, Hefei, Anhui 230601, P. R. China

[b]School of Physics and Materials Science, Anhui University, Hefei, Anhui, 230601, P. R. China.

[c]Anhui Province Key Laboratory of Chemistry for Inorganic/Organic Hybrid Functionalized Materials, Hefei, Anhui, 230601, P. R. China.

*Corresponding author. E-mails: clj@ustc.edu; yyq@ahu.edu.cn

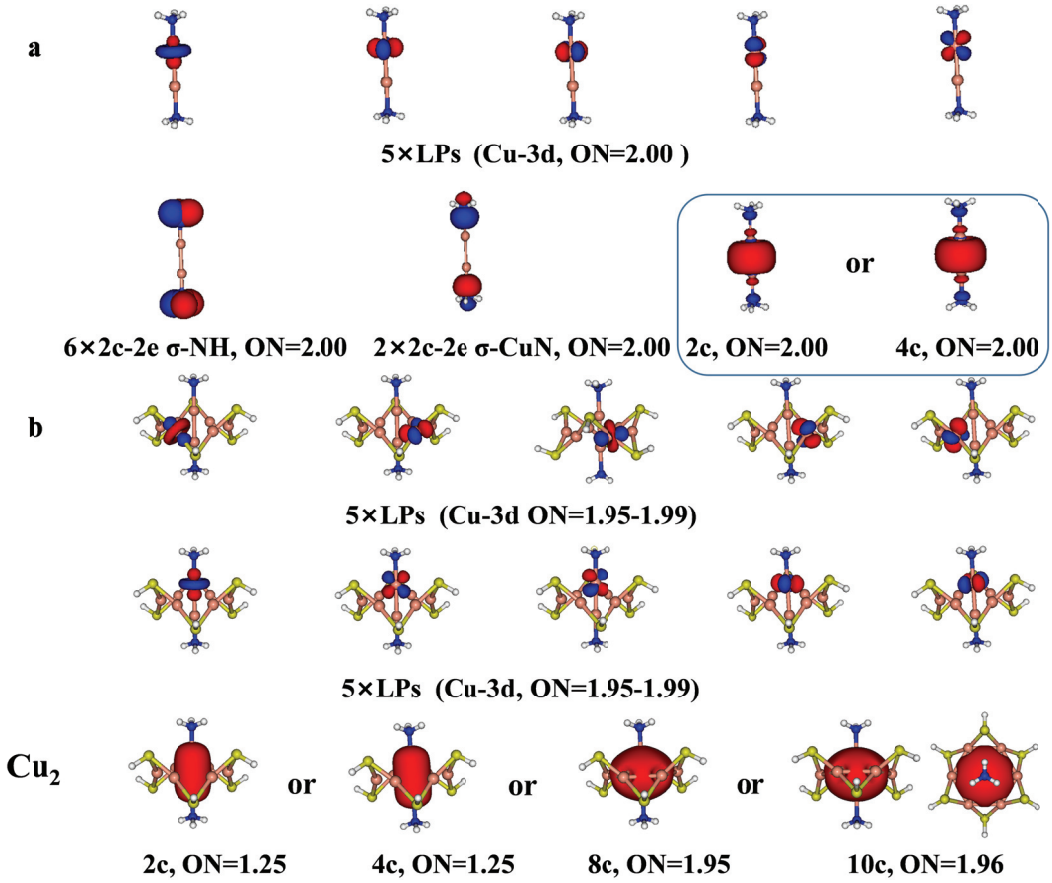

Fig. S1 AdNDP chemical bonding analysis for the (a) $(CuNH_3)_2$ monomer and (b) $(CuL)_2$@$(CuSH)_6$ (L=NH_3) complex (TPSS-D3/def2-tzvp). ON gives the occupancy number.

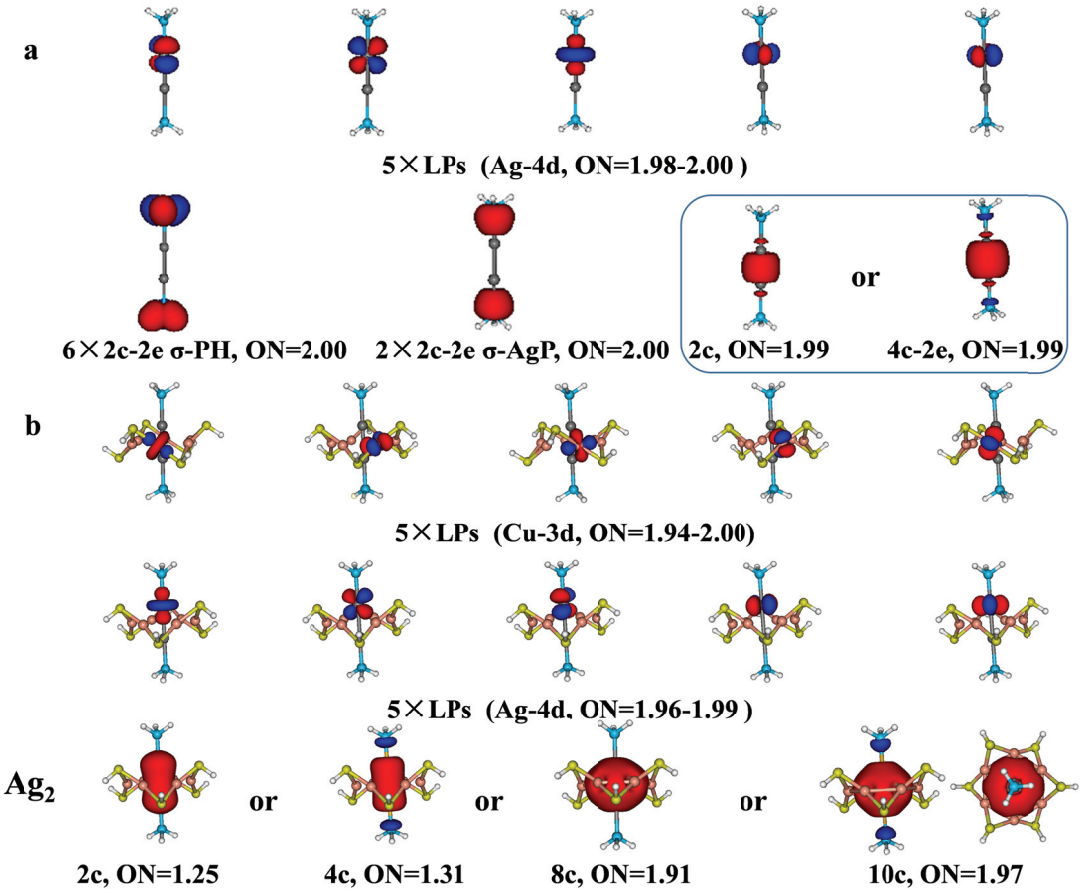

Fig. S2 AdNDP chemical bonding analysis for the (a) $(AgL)_2$ monomer and (b) $(AgL)_2@(CuSH)_6$ (L=PH_3) complex.

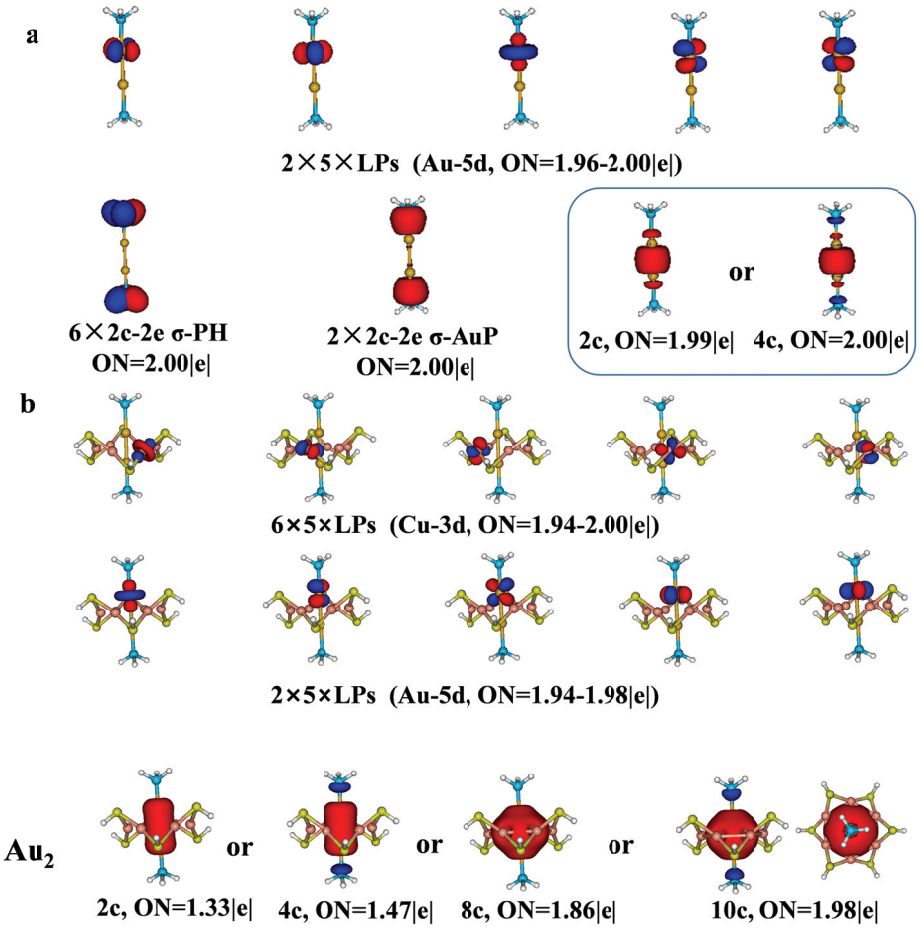

Fig. S3 AdNDP chemical bonding analysis for the (a) $(AuL)_2$ monomer and (b) $(AuL)_2@(CuSH)_6$ (L=PH_3) complex.

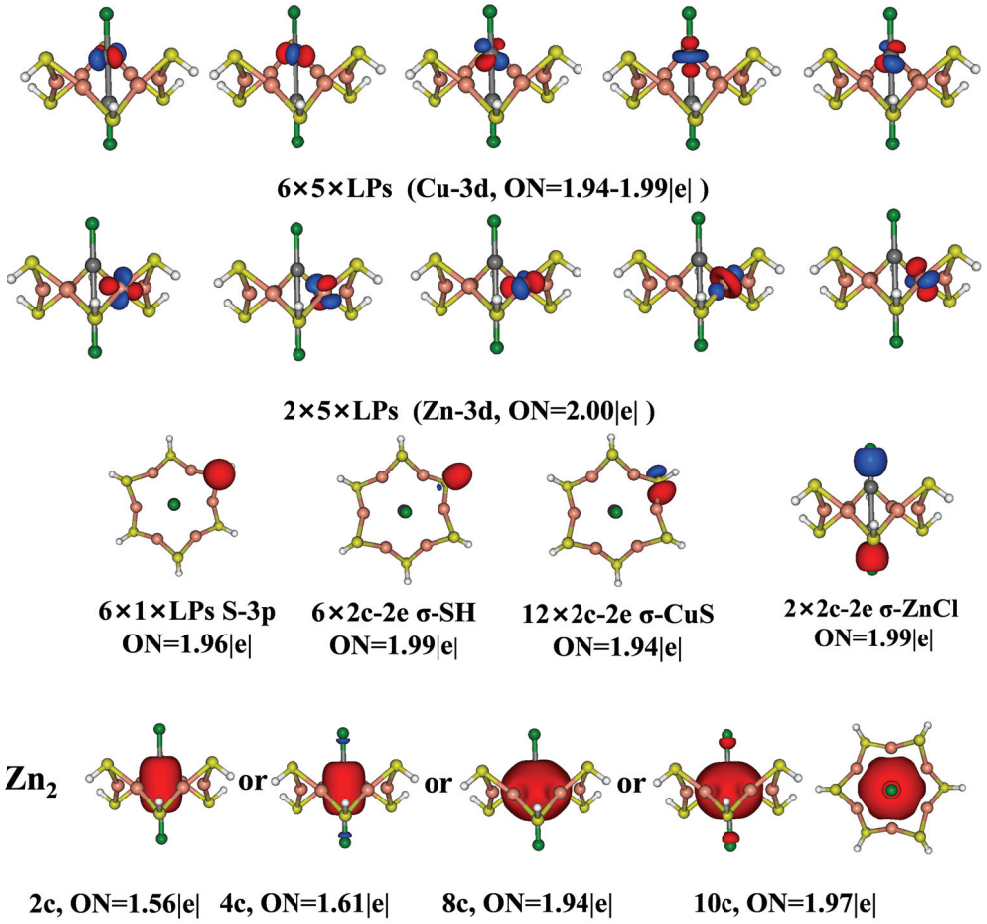

Fig. S4 AdNDP chemical bonding analysis for the $(ZnL)_2$@$(CuSH)_6$ (L=Cl) complex.

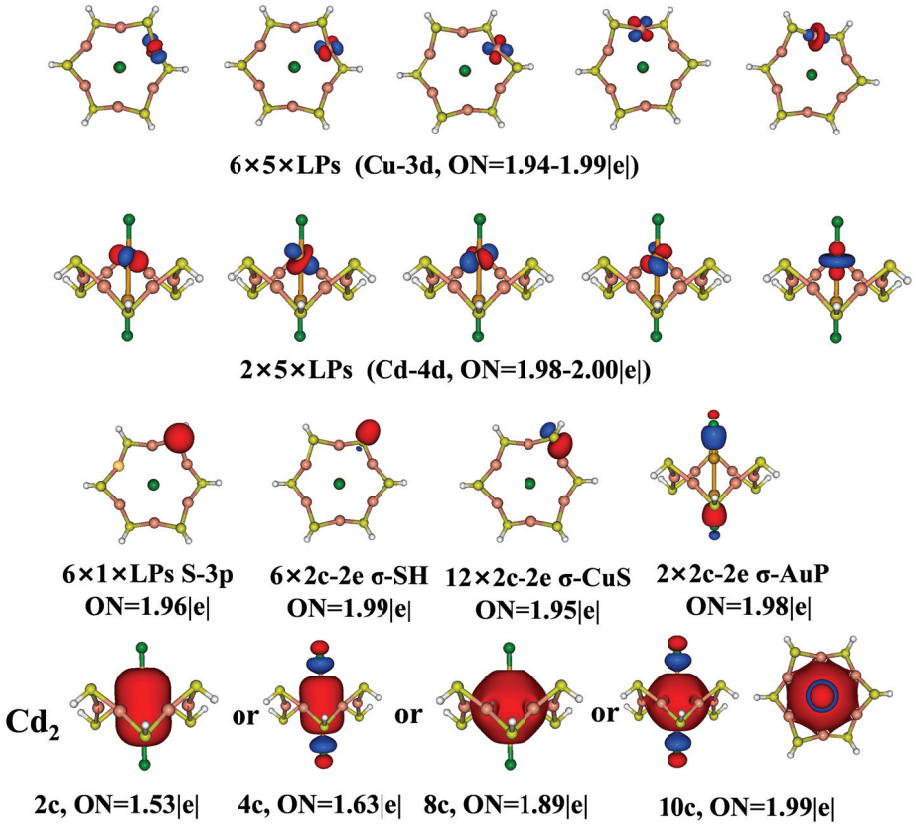

Fig. S5 AdNDP chemical bonding analysis for the $(CdL)_2@(CuSH)_6$ (L=Cl) complex

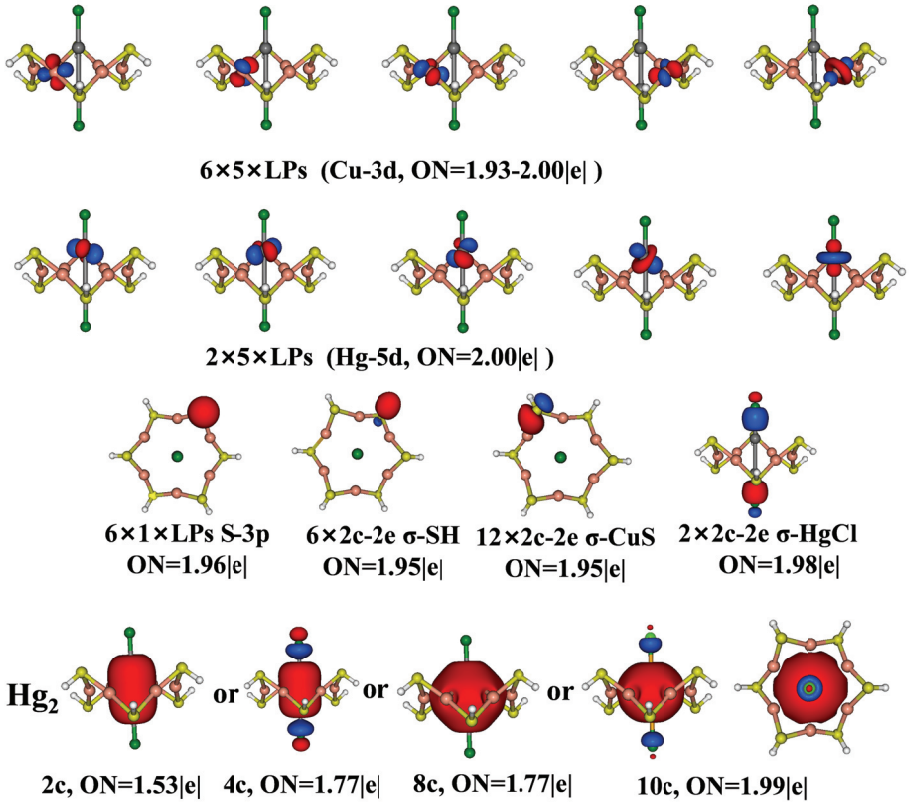

Fig. S6 AdNDP chemical bonding analysis for the $(HgL)_2@(CuSH)_6$ (L=Cl) complex.